Efficient and Accurate Registration of Point Clouds with Plane to Plane Correspondences

Wolfgang Förstner
Institute of Geodesy and Geoinformation
University of Bonn, Germany
wf@ipb.uni-bonn.de

Kourosh Khoshelham
Department of Infrastructure Engineering
The University of Melbourne, Australia
k.khoshelham@unimelb.edu.au

Abstract

We propose and analyse methods to efficiently register point clouds based on plane correspondences. This is relevant in man-made environments, where most objects are bounded by planar surfaces. Based on a segmentation of the point clouds into planar regions and matches of planes in different point clouds, we (1) optimally estimate the relative pose(s); (2) provide three direct solutions, of which two take the uncertainty of the given planes into account; and (3) analyse the loss in accuracy of the direct solutions as compared to the optimal solution. The paper presents the different solutions, derives their uncertainty especially of the suboptimal direct solutions, and compares their accuracy based on simulated and real data. We show that the direct methods that exploit the uncertainty of the planes lead to a maximum loss of 2.76 in accuracy of the estimated motion parameters in terms of the achieved standard deviations compared to the optimal estimates. We also show that the results are more accurate than the classical iterative closest point and iterative closest plane method, but the estimation procedures have a significantly lower computational complexity. We finally show how to generalize the estimation scheme to simultaneously register multiple point clouds.[1]

[1]The second author currently is with the Lyles School of Civil Engineering, Purdue University, West Lafayette, USA

1. Introduction

Registering 3D point clouds captured by various range cameras and laser scanners is an imprtant task in mapping natural and man-made environments. The registration involves finding corresponding elements in two point clouds and estimating a rigid motion using the correspondences. This process is often expensive and inefficient, particularly for large point clouds containing billions of points. In addition, existing methods for estimating the motion do not fully exploit the uncertainty of the points, resulting in suboptimal estimates of the motion parameters.

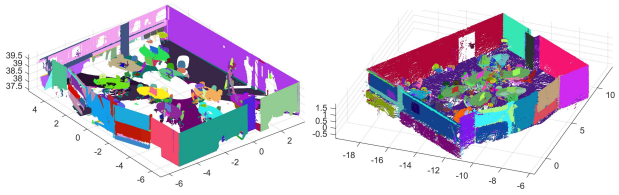

Figure 1: Segmented point clouds captured by a terrestrial laser scanner (TLS), containing 4.431 million points in 269 planar segments (left), and a Zeb sensor, containing 1.525 million points in 261 planar segments (right). The ceilings have been removed for better visualization of the interior. We propose and analyse efficient optimal and suboptimal methods for determining the relative motion between the two data sets based on plane-to-plane correspondences

Existing methods for point cloud registration can be classified according to the type of correspondences used for motion estimation. Point-to-point correspondences are by far the most common. The classical iterative closest point algorithm (ICP) [2] estimates the motion parameters by minimizing Euclidean distances between point correspondences. The motion estimation is, however, suboptimal, as corresponding points in the two sets usually do not refer to the same scene point. Maier-Hein et al. [18] and Bilings et al. [3] propose methods for improving the ICP by incorporating the measurement noise in the motion estimation.

The well known point-to-plane ICP [5] estimates the motion parameters by minimizing the orthogonal distance between the points in one point cloud and the corresponding local planes in the other. It does not require that the points, which carry the tangent plane, correspond to a point in the other data set. The motion estimation in the original ICP and other similar methods that use point-to-plane correspondences [19, 17, 23, 14] do not involve the uncertainty of the points and local planes, and is therefore suboptimal. The generalized ICP proposed by Segal et al. [26] allows for the inclusion of arbitrary covariance matrices in both point-to-point and point-to-plane variants of ICP.

A general drawback of the point-to-point and point-to-plane ICP algorithm is the expensiveness of the iterative search for correspondences. Unlike the point-to-

point and point-to-plane correspondences, motion estimation from plane-to-plane correspondences is very efficient [11, 4, 13]. This approach is relevant in man-made environments, where structures with large planar surfaces are abundant. Point cloud segmentation into planar segments can be done very efficiently [30, 29], even in real time [12], and once the corresponding planes are found, which can be supported by matched 3D lines [1], motion parameters can be estimated efficiently without needing to update the correspondences [22]. Pathak et al. [21, 20] propose methods for the estimation of plane uncertainties based on a radial noise model, which is applicable to only a few types of range sensors. The challenge in plane-to-plane registration, which has not been properly addressed before, is to exploit the uncertainty to obtain an optimal estimate of the motion based on an appropriate representation of uncertain planes.

In this paper, we present an optimal solution and three direct solutions for efficient motion estimation from plane-to-plane correspondences. We provide an analysis of the accuracy of the solutions, and compare their performance with the classical iterative closest point (ICP) algorithm. We show that our solutions yield motion estimates that are more accurate than the ICP method, but at the same time have a significantly lower computational complexity.

The paper proceeds with the representation of uncertain planes and the method for optimal motion estimation from uncertain plane pairs in Section 2. The three direct solutions are derived in Section 3, and the results of emprirical evaluation are presented in Section 4. Extending the methods to registeration of multiple point clouds is discussed in Section 5, followed by outlook and future research in Section 6.

2. The Task

We address the following task: Given are two 3D point clouds represented in two frames which are related by a motion $\mathcal{M}(\boldsymbol{R}, \boldsymbol{T})$. We assume the point clouds are segmented into two sets of planar patches, see Figure 1, and a set of I corresponding planar patches $\{\mathcal{A}, \mathcal{A}'\}_i, i = 1, ..., I$ has been identified. The task is to find a best estimate $\widehat{M}\{\widehat{R}, \widehat{T}\}$ for the motion between the two frames. We first present a maximum likelihood (ML) estimate for the motion parameters, and then three different direct solutions with different degrees of approximation.

The optimal solution assumes we have information about the uncertainty of the planes observed in the two frames. We specifically assume the plane pairs are mutually independent, a condition which can be relaxed, see Section 5, and the covariance matrix of the plane parameters is sufficient to describe their uncertainty. We will first provide the different representations for the uncertain planes, and how they are derived from the point cloud: based on the constraints between the plane pairs and the unknown motion we derive maximum likelihood estimates for the motion parameters.

2.1. Representing uncertain planes and motions

A plane has three degrees of uncertainty: two referring to the direction of the normal $\boldsymbol{N}$ and one referring to the position of the plane in the direction of the normal. We use two different representations, which are useful for different purposes.

Uncertain planes from 3D points. We start from the centroid representation, which evolves, when estimating the parameters $\mathbf{A}$ of plane $\mathcal{A}$ form 3D points $\boldsymbol{X}_j, j = 1, ..., J$.[2] Assuming the coordinates of the points are mutually independent and have a common standard deviation σ, we can optimally estimate the plane parameters. We use the weighted centroid $\boldsymbol{X}_0 = \sum_j \boldsymbol{X}_j / J$ and the scatter matrix $\sum_j (\boldsymbol{X}_j - \boldsymbol{X}_0)(\boldsymbol{X}_j - \boldsymbol{X}_0)^\mathsf{T}$ with its eigenvalue decomposition $\boldsymbol{Q}\boldsymbol{\Lambda}\boldsymbol{Q}^\mathsf{T}$. The eigenvector belonging to the smallest eigenvalue (λ_3) is an estimate for the normal of the plane and the plane passes through the centroid.[3] We then obtain the variance σ_q^2 of the position of the plane along the normal, and the principal variances σ_ϕ^2 and σ_ψ^2 of the direction of the normal from the eigenvalues $\lambda_1 \geq \lambda_2 \geq \lambda_3$ via the estimated variance of the 3D points $\widehat{\sigma}^2 = \lambda_3 / J$ and thus

$$\widehat{\sigma}_q^2 = \widehat{\sigma}^2 / J \qquad \widehat{\sigma}_\phi^2 = \widehat{\sigma}^2 / \lambda_1 \qquad \widehat{\sigma}_\psi^2 = \widehat{\sigma}^2 / \lambda_2 \,. \tag{1}$$

Hence we generally can represent an uncertain plane by the tuple

$$\underline{\mathcal{A}}: \quad \{\boldsymbol{X}_0, \boldsymbol{Q}; \sigma_\phi, \sigma_\psi, \sigma_q\} \,, \tag{2}$$

where estimates of the parameters are used in practical cases. Planes derived from 3D points with arbitrary covariance matrix also can be represented this way, see [9, (10.62)].

We now can easily determine the homogeneous coordinates $\mathbf{A}^e = [\boldsymbol{N}^\mathsf{T}, -S]^\mathsf{T}$ of the uncertain plane $\mathcal{A}$ in general position, with its normal $\boldsymbol{N}$ and its distance S to the origin.[4] We start from the uncertain plane with its mean at $\mathcal{A}_0(\mathbf{A}_0)$, its centroid at $\mathbf{0}$, its axes $\boldsymbol{Q} = \boldsymbol{I}_3$, hence $\mathbf{A}_0 = [0, 0, 1, 0]^\mathsf{T}$, and its covariance matrix $\Sigma_{A_0 A_0} = \mathrm{Diag}([\sigma_\phi^2, \sigma_\psi^2, 0, \sigma_q^2])$. We move this plane $\mathcal{A}_0$ to $\mathcal{A}$ via $\mathsf{M}^{-\mathsf{T}}(\boldsymbol{Q}, \boldsymbol{X}_0)\mathbf{A}_0$ and normalize it thus $\mathbf{A}^e = \mathsf{N}^e(\mathbf{A}) := \mathbf{A}/\sqrt{A_1^2 + A_2^2 + A_3^2}$. By variance propagation we first obtain the covariance matrix $\Sigma_{AA} = \mathsf{M}^{-\mathsf{T}} \Sigma_{A_0 A_0} \mathsf{M}^{-1}$ of the homogeneous coordinates of the moved plane $\mathsf{M}^{-\mathsf{T}}(\boldsymbol{Q}, \boldsymbol{X}_0)\mathbf{A}_0$. The covariance matrix of the normalized plane coordinates $\mathbf{A}^e = [\boldsymbol{N}^\mathsf{T}, -S]^\mathsf{T}$ is $\Sigma_{A^e, A^e} = \boldsymbol{J}_e(\mathbf{A}) \Sigma_{AA} \boldsymbol{J}_e^\mathsf{T}(\mathbf{A})$ with the Jacobian

$$\boldsymbol{J}_e(\mathbf{A}) = \frac{\partial \mathbf{A}^e}{\partial \mathbf{A}} = \frac{1}{\sqrt{A_1^2 + A_2^2 + A_3^2}} \begin{bmatrix} \boldsymbol{I}_3 - \boldsymbol{N}\boldsymbol{N}^\mathsf{T} & \mathbf{0} \\ S\boldsymbol{N}^\mathsf{T} & 1 \end{bmatrix} . \tag{3}$$

[2] We reserve the index i for planes.

[3] If the points have different weight $w_j = 1/\sigma_j^2$, this can be taken into account by weighting. Only if the uncertainty of the 3D points is not isotropic, the estimation of the optimal plane is more involving.

[4] The superscript ^{e} stands for Euclidean normalization.

In the following we simplify notation, and assume homogeneous plane coordinates $\mathbf{A}$ *are normalized such that* $A_1^2 + A_2^2 + A_3^2 = 1$*, thus omit the superscript* ^{e}.

Uncertain motions. Following [6], an uncertain motion $\underline{\mathcal{M}}$ is represented by $\{\boldsymbol{\mu}_{\mathsf{M}}, \Sigma_{\xi\xi}\}$,[5] thus its mean and the covariance matrix of the random twist vector $\underline{\boldsymbol{\xi}} = [\underline{\boldsymbol{r}}^\mathsf{T}, \underline{\boldsymbol{t}}^\mathsf{T}]^\mathsf{T}$, where

$$\underline{\mathsf{M}} = \exp(K(\underline{\boldsymbol{\xi}}))\boldsymbol{\mu}_{\mathsf{M}} \approx (I_4 + K(\underline{\boldsymbol{\xi}}))\boldsymbol{\mu}_{\mathsf{M}} \tag{4}$$

or $\underline{\mathsf{M}} = \mathsf{M}(R(\underline{\boldsymbol{r}}), \underline{\boldsymbol{t}})\boldsymbol{\mu}_{\mathsf{M}}(\boldsymbol{\mu}_R, \boldsymbol{\mu}_T)$. The random twist vector $\boldsymbol{\xi}$, thus collects the small rotation vector $\boldsymbol{r}$ and the small translation vector $\boldsymbol{t}$. Then we have for small $\boldsymbol{r}$

$$\exp(K(\boldsymbol{\xi})) = \exp\left(\begin{bmatrix} S(\boldsymbol{r}) & \boldsymbol{t} \\ \mathbf{0}^\mathsf{T} & 1 \end{bmatrix}\right) \approx^{6} \begin{bmatrix} R(\boldsymbol{r}) & \boldsymbol{t} \\ \mathbf{0}^\mathsf{T} & 1 \end{bmatrix}, \tag{5}$$

where the rotation matrix can be determined from Rodriguez' form $R(\boldsymbol{r}) = ((4+||\boldsymbol{r}||^2)I + 4S(\boldsymbol{r}) + 2S^2(\boldsymbol{r}))/(4+||\boldsymbol{r}||^2)$, with the skew matrix $S(\boldsymbol{r})$ of the 3-vector $\boldsymbol{r}$.

2.2. The constraints

If points with homogeneous coordinates $\mathbf{X}$ are transformed according to $\mathbf{X}' = \mathsf{M}\mathbf{X}$ then the 3D planes with homogeneous coordinates $\mathbf{A}$ are transformed according to $\mathbf{A}' = \mathsf{M}^{-\mathsf{T}}\mathbf{A}$, thus we have the back projection $\mathbf{A} = \mathsf{M}^\mathsf{T}\mathbf{A}'$.[7] Assuming the planes are not at infinity we therefore can use the constraint between the observed plane pair $(\mathbf{A}, \mathbf{A}')$ and the motion $(R, \boldsymbol{T})$

$$\mathbf{0} = R\boldsymbol{N} - \boldsymbol{N}' \quad \text{and} \quad 0 = \boldsymbol{N}'^\mathsf{T}\boldsymbol{T} - S + S'. \tag{6}$$

Only three of these four constraints are independent, since the identity of two normals, in the first expression, only requires two constraints. We only need to compare their direction. This can be achieved by comparing the position of $R\boldsymbol{N}$ and $\boldsymbol{N}'$ on the unit sphere S^2, by projecting the normals to the tangent space at $\boldsymbol{N}'$, spanned by a basis of the nullspace of $\boldsymbol{N}'^\mathsf{T}$ see the minimal representation of the normal in the Supplement and [9, Sect. 10.2.2]. Thus the we have the two constraints

$$J_r^\mathsf{T}(\boldsymbol{\mu}_{N'})(R\widehat{\boldsymbol{N}} - \widehat{\boldsymbol{N}}') = \mathbf{0} \;\text{ with }\; J_r(\boldsymbol{N}') = \text{null}(\boldsymbol{N}'^\mathsf{T}) \tag{7}$$

for the normal. The three necessary constraints for two planes $\mathbf{A}$ and $\mathbf{A}$ matching after motion M finally are

$$\mathbf{0} = \boldsymbol{g}(\mathsf{M}; \mathbf{A}, \mathbf{A}') := \begin{bmatrix} J_r^\mathsf{T}(\boldsymbol{\mu}_{N'})(R\widehat{\boldsymbol{N}} - \widehat{\boldsymbol{N}}') \\ \widehat{\boldsymbol{N}}'^\mathsf{T}\boldsymbol{T} - \widehat{S} + \widehat{S}' \end{bmatrix}. \tag{8}$$

[5] Random variables are underscored.

[6] We have the upper right element $V(\boldsymbol{r})$ of $\exp(K(\underline{\boldsymbol{\xi}}))$ generally: $V(\boldsymbol{r}) = I_3 + \sum_{n=1}^{\infty} S^n(\boldsymbol{r})/(n+1)!$, which simplifies to $\boldsymbol{t}$ for small $\boldsymbol{r}$, see [6]

[7] Equality relations for homogeneous entities hold up to scale.

2.3. The ML-estimation

The plane parameters $\mathbf{A}$ and $\mathbf{A}'$ are observed, therefore the constraints will not be fulfilled. Taking their uncertainty into account we perform a maximum-likelihood estimation leading to best estimates $\widehat{\mathbf{A}}$ and $\widehat{\mathbf{A}}'$ for the planes and $\widehat{\mathsf{M}}$ for the motion. Hence, we assume the constraints $\boldsymbol{g}$ hold for these estimated values. Since the motion M is unknown, and the constraints are nonlinear we assume to have approximate values $\widehat{\mathbf{A}}^a$, $\widehat{\mathbf{B}}^a$, and $\widehat{\mathsf{M}}^a$ for the final estimates. This estimation needs to take into account the special structures of the plane parameters, namely that the normals are unit vectors, and of the motion matrix, namely that it contains a rotation matrix. This we realize by estimating a minimal set of parameters for the planes and the motion.

Using the minimal representation for the normal we have the following relations, for the plane $\mathbf{A}$

$$\widehat{\mathbf{A}} = \begin{bmatrix} \mathsf{N}(\widehat{\mathbf{N}}^a + J_r(\widehat{\mathbf{N}}^{a\mathsf{T}})\widehat{\Delta\boldsymbol{N}}_r) \\ -(S^a + \widehat{\Delta S}) \end{bmatrix} \tag{9}$$

$$= \begin{bmatrix} \mathsf{N}(\widehat{\mathbf{N}}^a + J_r(\widehat{\mathbf{N}}^{a\mathsf{T}})(\boldsymbol{N}_r + \widehat{\boldsymbol{v}}_{N_r})) \\ -(S + \widehat{v}_S) \end{bmatrix}. \tag{10}$$

Here, using the estimated residuals $\widehat{\boldsymbol{v}}_{A_r}$ and the corrections $\widehat{\Delta\boldsymbol{A}}_r$ for the reduced plane parameters

$$\widehat{\boldsymbol{v}}_{A_r} = \begin{bmatrix} \widehat{\boldsymbol{v}}_{N_r} \\ \widehat{v}_S \end{bmatrix} \quad \text{and} \quad \widehat{\Delta\boldsymbol{A}}_r = \begin{bmatrix} \widehat{\Delta\boldsymbol{N}}_r \\ \widehat{\Delta S} \end{bmatrix}, \tag{11}$$

we exploited the two expressions for the fitted observations $\widehat{\boldsymbol{A}}_r = \boldsymbol{A}_r + \widehat{\boldsymbol{v}}_{A_r} = \widehat{\boldsymbol{A}}_r^a + \widehat{\Delta\boldsymbol{A}}_r$, taking into account $\widehat{\boldsymbol{N}}_r^a = \mathbf{0}$. The expressions for the plane $\mathbf{A}'$ are similar. For the motion we have up to first order terms $\mathsf{M} = \widehat{\mathsf{M}}^a + K(\widehat{\Delta\boldsymbol{\xi}})\widehat{\mathsf{M}}^a$, see (4). Hence, taking all plane pairs into account, the goal is to find the minimum of the weighted Mahalanobis distance of all residuals

$$\Omega\left(\widehat{\Delta\boldsymbol{\xi}}; \left\{\widehat{\Delta\boldsymbol{A}}_{ri}, \widehat{\Delta\boldsymbol{A}'}_{ri}\right\}\right) = \sum_{B\in\{A,A'\}} \sum_i ||\widehat{\boldsymbol{v}}_{B_{ri}}||^2_{\Sigma_{B_{ri}B_{ri}}} \tag{12}$$

such that the constraints (8) for the fitted values are fulfilled, see [9, Sect. 10.6.1].

The weighting of the residuals, *e.g.* by $||\widehat{\boldsymbol{v}}_{A_{ri}}||^2_{\Sigma_{A_{ri}A_{ri}}} = \widehat{\boldsymbol{v}}^\mathsf{T}_{A_{ri}}\Sigma^{-1}_{A_{ri}A_{ri}}\widehat{\boldsymbol{v}}_{A_{ri}}$ by the inverse covariance matrix allows to exploit the information of the plane generation process, see Section 2.1, by tracking the uncertainty $\Sigma_{X_jX_j}$ from the given 3D points $\mathcal{X}_j$ through the uncertainty of the planes $\Sigma_{A_iA_i}$ to the uncertainty $\Sigma_{\widehat{\xi}\widehat{\xi}}$ of the estimated motion. We assume the observations are given together with the covariance matrix of their reduced coordinates:

$$\boldsymbol{y}_i = \begin{bmatrix} \mathbf{A}_{ri} \\ \mathbf{A}'_{ri} \end{bmatrix} \text{ with } \Sigma_{y_iy_i} = \sigma_0^2 \begin{bmatrix} \Sigma_{A_{ri}A_{ri}} & \\ & \Sigma_{A'_{ri}A'_{ri}} \end{bmatrix}. \tag{13}$$

Thus the uncertainty is known up to an unknown variance factor σ_0^2 which can be estimated from the data.

The iterative solution starts from approximate values for the fitted planes and the motion and performs updates for the motion parameters derived from the normal equations $N\Delta\boldsymbol{\xi} = \boldsymbol{n}$, and updates for the plane parameters $\widehat{\mathbf{A}}$ and $\widehat{\mathbf{A}}'$ following (9). After convergence we obtain the theoretical covariance matrix

$$\Sigma_{\widehat{\xi}\widehat{\xi}}(\boldsymbol{g}, \Sigma_{yy}) = N^{-1}\,, \tag{14}$$

which is the Cramer-Rao bound. This covariance matrix is close to the empirical uncertainty of the estimated parameters, if the model is fulfilled, *i.e*. the plane correspondences hold and their uncertainty is reflected in the covariances, and the noise is not too large, such that the applied first order approximations are acceptable. Using simulated data, we therefore can check whether the simulation of the data and the estimation procedure are consistent. The covariance matrix only depends on the assumptions about the constraints $\boldsymbol{g}$ and the uncertainty Σ_{yy} of the observations, not on the actual observations. The estimated variance factor

$$\underline{\widehat{\sigma}_0}^2 = \underline{\Omega}/R \sim F(R, \infty) \quad \text{with} \quad R = G - U \tag{15}$$

can be used for checking the consistency of data and model. The number of degrees of freedom is identical to the redundancy $R = G - U = 3I - 6$ of the estimation problem.

In case the percentage of wrong plane-plane correspondences is not too large, using maximum-likelihood type robust estimation allows to find to eliminate the outliers and reach the correct (global) optimum, see [8, 31]. Applying a gradient non-convexity iteration scheme, as in [31], speeds up the procedure.

3. Direct solutions

The maximum likelihood estimation procedure is iterative and requires approximate values, especially for the motion. We therefore need a direct solution for determining the motion parameters. Usually direct solutions are accurate enough for guaranteeing convergence, however, are statistically suboptimal. We discuss three direct solutions. Two of them take the uncertainty of the given plane parameters into account and, as will be shown, lead to results very close to the maximum likelihood solution:

(1) an algebraic solution proposed by [14]. This solution estimates rotation and translation separately and does not exploit the uncertainty of the given plane pairs. We will refer to this solution as ALG.

Two two-step procedures which use the algebraic solution as first step and exploit the uncertainty of the given plane pairs in the second step:

(2) a whitened version of the algebraic solution, together with the algebraic solution indicated with ALGW. This solution still estimates rotation and translation separately, and

(3) the first iteration of an ML solution, together with the algebraic solution indicated with ML-1. This solution determines the Jacobians at the observed, instead of the fitted values.

We expect the three solutions to yield results which are increasingly closer to the optimal ML estimation.

We derive covariance matrices for the first two solutions.

3.1. The direct algebraic solution

The direct solution, proposed by [14], observes, that the two sets of constraints in (8) allow to separately estimate the rotation and the translation.

The first expression contains two linearly independent constraints and only relates to the rotation. It refers to the estimated parameters and fitted observations. If we use the observed normals $\boldsymbol{N}'_i$ instead of their mean value for determining the Jacobian, we arrive at the residual vector

$$\boldsymbol{g}_{i,r} = J_r^\mathsf{T}(\boldsymbol{N}'_i)R\boldsymbol{N}_i = (\boldsymbol{N}_i^\mathsf{T} \otimes J_r^\mathsf{T}((\boldsymbol{N}'_i)))\ \mathrm{vec}R \tag{16}$$

The estimate, $\widehat{R} = \mathrm{argmin}_R\ ||\boldsymbol{g}_r||^2$, for the rotation which minimizes the algebraic error $||\boldsymbol{g}_r|| = |||[\boldsymbol{g}_{i,r}]|||$ can be found as the right singular vector of the matrix $[(\boldsymbol{N}_i^\mathsf{T} \otimes J_r^\mathsf{T}((\boldsymbol{N}'_i)))]$ belonging to the smallest singular value $\mathrm{vec}(\widehat{R}) = V(:, 9)$ with $[(\boldsymbol{N}_i^\mathsf{T} \otimes J_r^\mathsf{T}((\boldsymbol{N}'_i)))] = UDV^\mathsf{T}$. Since the orthogonality of $\widehat{R}$ is not enforced we finally obtain the estimate from

$$\widehat{R}^{\mathrm{ALG}} = UV^\mathsf{T} \quad \text{with} \quad \widehat{R} = UDV^\mathsf{T}\,. \tag{17}$$

The translation can directly be derived by minimizing the residuals $\boldsymbol{g}_t = [\boldsymbol{g}_{i,t}] = [{\boldsymbol{N}_i}'^\mathsf{T}\boldsymbol{T} - S_i + S'_i]$, hence by $\widehat{\boldsymbol{T}}^{\mathrm{ALG}} = \mathrm{argmin}_T\ ||\boldsymbol{g}_t||^2$. Since the unknown parameters $\boldsymbol{T}$ occur quadratically in the minimization function we obtain them from the linear equation system

$$\widehat{\boldsymbol{T}}^{\mathrm{ALG}} = (X^\mathsf{T}X)^{-1}X^\mathsf{T}\boldsymbol{y}\,. \tag{18}$$

with $X = [{\boldsymbol{N}_i}'^\mathsf{T}]$ and $\boldsymbol{y} = [S_i - S'_i]$

The Covariance Matrix of the Solution

The solution is suboptimal. Still, we can derive its covariance matrix by implicit variance propagation.

Let the constraint between the non-reduced observations

$$\underset{1\times 8}{\boldsymbol{y}_i^\mathsf{T}} := [\mathbf{A}_i^\mathsf{T}, {\mathbf{A}_i}'^\mathsf{T}] = [\boldsymbol{N}_i^\mathsf{T} - S_i, {\boldsymbol{N}_i}'^\mathsf{T} - S'_i] \tag{19}$$

with their 8×8 covariance matrix $\mathrm{Diag}([\Sigma_{A_iA_i}, \Sigma_{A'_iA'_i}])$, and the parameters $\boldsymbol{\beta} = \{R, \boldsymbol{T}\}$ have the form $\mathbf{0} = \boldsymbol{g}(\widehat{\boldsymbol{\beta}}, \widehat{\boldsymbol{y}}) = [\boldsymbol{g}_i(\widehat{\boldsymbol{\beta}}, \widehat{\boldsymbol{y}}_i)]$. We linearize with $\Delta\boldsymbol{\beta} := \boldsymbol{\xi} = [\boldsymbol{r}^\mathsf{T}, \boldsymbol{t}^\mathsf{T}]^\mathsf{T}$

$$\Delta\boldsymbol{g}(\boldsymbol{\beta}, \boldsymbol{y}) = X\boldsymbol{\xi} + Z^\mathsf{T}\Delta\boldsymbol{y} = \mathbf{0}\,. \tag{20}$$

Therefore the (corrections to the) unknown parameters are $\widehat{\boldsymbol{\xi}} = -\boldsymbol{X}^{+}\boldsymbol{Z}^{\mathsf{T}}\Delta\boldsymbol{y}$. This leads to the covariance matrix

$$\Sigma_{\widehat{\xi}\widehat{\xi}} = \boldsymbol{X}^{+}\boldsymbol{Z}^{\mathsf{T}}\Sigma_{yy}\boldsymbol{Z}\boldsymbol{X}^{+} \tag{21}$$

In our special case we have the Jacobians $\underset{3I\times 6}{\boldsymbol{X}} = [\boldsymbol{X}_i^{\mathsf{T}}]$ and $\underset{3I\times 8I}{\boldsymbol{Z}^{\mathsf{T}}} = \mathrm{Diag}([\boldsymbol{Z}_i^{\mathsf{T}}])$ with

$$\underset{3\times 6}{\boldsymbol{X}^{\mathsf{T}}} = \begin{bmatrix} -\boldsymbol{J}_r^{\mathsf{T}}(\boldsymbol{N}')\boldsymbol{S}(\boldsymbol{R}^a\boldsymbol{N}) & \boldsymbol{0} \\ \boldsymbol{0}^{\mathsf{T}} & \boldsymbol{N}'^{\mathsf{T}} \end{bmatrix} \tag{22}$$

$$\underset{3\times 8}{\boldsymbol{Z}^{\mathsf{T}}} = \begin{bmatrix} \boldsymbol{J}_r^{\mathsf{T}}(\boldsymbol{N}')\boldsymbol{R}^a & \boldsymbol{0} & -\boldsymbol{J}_r(\boldsymbol{N}') & \boldsymbol{0} \\ \boldsymbol{0}^{\mathsf{T}} & -1 & \boldsymbol{T}^{a\mathsf{T}} & 1 \end{bmatrix} \tag{23}$$

With $\boldsymbol{S} = \sum_i \boldsymbol{X}_i\boldsymbol{X}_i^{\mathsf{T}}$ we therefore have

$$\Sigma_{\widehat{\xi}\widehat{\xi}}^{\mathrm{ALG}} = \boldsymbol{S}^{-1}\left(\sum_i \boldsymbol{X}_i\boldsymbol{Z}_i^{\mathsf{T}}\Sigma_{y_iy_i}\boldsymbol{Z}_i\boldsymbol{X}_i^{\mathsf{T}}\right)\boldsymbol{S}^{-1}. \tag{24}$$

3.2. The direct whitened algebraic solution

The algebraic solution is suboptimal for two reasons: (1) the uncertainty of the given planes is not exploited, (2) the solution depends on the observed, not on the fitted observations.

We can exploit the uncertainty of the observed planes in the following manner, which can be applied to all algebraic solutions and is a generalization of the method of [27], here including the different uncertainties of the given observations. The algebraic errors $\boldsymbol{g}_i(\boldsymbol{R}, \boldsymbol{T}; \boldsymbol{y}_i)$ depend on the observations and do not have the same covariance matrix, when assuming the motion parameters are fixed. Instead of minimizing the algebraic error we minimize the Mahalanobis distance of these errors $\boldsymbol{g} = [\boldsymbol{g}_i]$ to $\boldsymbol{0}$:

$$\{\widehat{\boldsymbol{R}}^{\mathrm{ALGw}}, \widehat{\boldsymbol{T}}^{\mathrm{ALGw}}\} = \mathrm{argmin}_{R,T}\ \boldsymbol{g}^{\mathsf{T}}\Sigma_{gg}^{-1}\boldsymbol{g}. \tag{25}$$

For this we use the covariance matrix of the algebraic errors $\Sigma_{g_ig_i} = \boldsymbol{Z}_i^{\mathsf{T}}\Sigma_{y_iy_i}\boldsymbol{Z}_i$ with $\boldsymbol{Z}_i^{\mathsf{T}} = \partial\boldsymbol{g}_i/\partial\boldsymbol{y}_i$.

The direct algebraic solution in our case performs a separate estimation of rotation and translation. If we whiten the rotation and the translation constraint separately, we use the covariance matrix of the rotation constraints

$$\underset{2\times 2}{\Sigma_{g_{i,r}g_{i,r}}} = \boldsymbol{Z}_{i,r}^{\mathsf{T}}\Sigma_{y_iy_i}\boldsymbol{Z}_{i,r}, \tag{26}$$

with $\boldsymbol{Z}_{i,r}^{\mathsf{T}}$ being the first two rows of $\boldsymbol{Z}_i$ in (23). The whitened rotation constraint therefore reads

$$\boldsymbol{J}_{ri}^{\mathsf{T}}\left(\boldsymbol{R}\widehat{\boldsymbol{N}}_i' - \widehat{\boldsymbol{N}}_i\right) = \boldsymbol{0} \quad \text{with} \quad \boldsymbol{J}_{ri} = \boldsymbol{J}_r(\boldsymbol{\mu}_{N_i})\Sigma_{g_{i,r}g_{i,r}}^{-1/2}. \tag{27}$$

Similarly, we have the variance of the translation constraint

$$\sigma_{g_{i,t}}^2 = \boldsymbol{Z}_{i,t}^{\mathsf{T}}\Sigma_{y_iy_i}\boldsymbol{Z}_{i,t} \ \text{ with } \ \boldsymbol{Z}_{i,t}^{\mathsf{T}} = [\boldsymbol{0}_{1\times 3}, -1, \widehat{\boldsymbol{T}}^{\mathrm{ALG},\mathsf{T}}, 1]. \tag{28}$$

and hence the whitened constraint for the translation

$$\left(\widehat{\boldsymbol{N}}_i'^{\mathsf{T}}\boldsymbol{T} - \widehat{S}_i + \widehat{S}_i'\right)/\sigma_{g_{i,t}} = 0. \tag{29}$$

The Covariance Matrix of the Whitened Algebraic Solution. Using the whitened constraints we can derive the covariance matrix $\Sigma_{\widehat{\xi}\widehat{\xi}}^{\mathrm{ALGw}}$ in the same manner as for the unwhitened constraints. We just have to take the Jacobians of these constraints; they result from (22) and (23) by substituting $\boldsymbol{J}_r$ by $\boldsymbol{J}_{rw}$ from (27) and $\boldsymbol{R}^a$ by $\boldsymbol{R}^{\mathrm{ALG}}$, and multiplying the last row of $\boldsymbol{Z}_i^{\mathsf{T}}$ by $1/\sigma_{g_{i,t}}$.

3.3. Single-iteration ML-solution

Instead of whitening the direct solution, we can arrive at a better approximate solution using the first iteration of an ML estimation taking the algebraically determined motion parameters as approximate values.

Starting from approximate values $\widehat{\boldsymbol{\xi}}^{\mathrm{ALG}}$ we obtain corrections $\widehat{\boldsymbol{\xi}}$ from the normal equations $\boldsymbol{N}\widehat{\boldsymbol{\xi}} = \boldsymbol{n}$ with the residuals of the constraints (8)

$$\boldsymbol{c}_g' = -\boldsymbol{g}(\widehat{\boldsymbol{\beta}}^{\mathrm{ALG}}, \boldsymbol{y}) := -[\boldsymbol{g}_i(\widehat{\mathsf{M}}^{\mathrm{ALG}}, \boldsymbol{y}_i)]. \tag{30}$$

evaluated at the approximate values $\widehat{\mathsf{M}}^{\mathrm{ALG}}$ of the algebraic solution and the observations $\boldsymbol{y}_i = [\mathbf{A}_i^{\mathsf{T}}, \mathbf{A}_i'^{\mathsf{T}}]^{\mathsf{T}}$, instead of the fitted observations (see [9, Eq. (4.444)]). These are not needed in this approximation and simplify the procedure.

Unfortunately, without knowing the rate of convergence no theoretical covariance matrix can be given. We however will see, that this second step often outperforms the whitened solution ALGw.

4. Empirical evaluation

We perform several empirical tests. First, we show, that the implemented estimation procedures yield the results they should, by performing decisive tests. Second, we compare the loss in accuracy of the suboptimal methods, when compared to the maximum likelihood estimates.

4.1. Correctness of the accuracy predictions

The maximum likelihood estimation procedure yields three results: the estimated parameters $\widehat{\boldsymbol{\xi}}$, their theoretical covariance matrix $\Sigma_{\widehat{\xi}\widehat{\xi}}$, and the estimated variance factor $\widehat{\sigma}_0^2$. The approximate methods do not yield a variance factor, and partly no covariance matrix. All three results can be tested statistically, see [9, Sect. 4.6.8]. If the test fires, there is an indication, that the simulation or the estimation method does not yield the desired results.

The tests are based on K repeated estimates, assuming the same true data and covariance matrices for the observations and adding noise to the observations, here the plane

pairs. In order to avoid second order effects, the tests are primarily performed with small standard deviations, *e.g.* below 0.01% of the average distance between the centroids of the planes. We will show, that for larger noise variances the statistical tests will fire, due to the neglection of higher order terms within the variance propagation.

The following tests refer to $I = 50$ planes pairs, with centroids randomly chosen in the cube $[-1, +1]^3$ and covariance matrices randomly chosen as $\Sigma_{A_{ri}A_{ri}} = \sigma_A^2(I_3 + UU^\mathsf{T})$, where U are random 3×3 matrices with $U_{kl} \sim \mathcal{N}(0, 1)$. The variances σ_A^2 of the planes $\mathcal{A}$ are assumed to be 9 times smaller than the variances $\sigma_{A'}^2$ of the planes $\mathcal{A}'$. The plots refer to the larger standard deviation.

Checking the correctness of the estimated noise level for ML-estimates. The estimated variance factor should be close to 1, if the generated observational data and the estimation model are consistent, *i.e.* their nominal values follow the constraints and the noise follows the assumed distribution, which is the null hypothesis. For testing we use the distribution $\underline{\widehat{\sigma_0}^2}|H_0 \sim F(R, \infty)$ of the estimated variance factor, where R is the redundancy of the estimation process, namely $R = G - U = 3I - 6$.

Figure 2, left, shows the histogram of $K = 300$ samples $\widehat{\sigma_{0,k}^2}$ of the variance factor, assuming $\sigma_A = 0.0003$: It visually fits the theoretical Fisher-distribution $F(R, \infty)$ with $R = 3 \times 50 - 6 = 144$. The mean value $\widehat{\sigma_0^2} = \sum_k \widehat{\sigma_{0,k}^2}/K = 0.99935$ is well in the 99.9% acceptance interval $[0.974, 1.027]$. Figure 2, right, shows the dependency of the estiamted variance factor as a function of the noise level: For noise levels below 1% the estimated variance factor does not significantly deviate from 1; for larger values the variance factor no longer follows a Fisher distribution with a suffient accuracy due to the nonlinearity of the model.

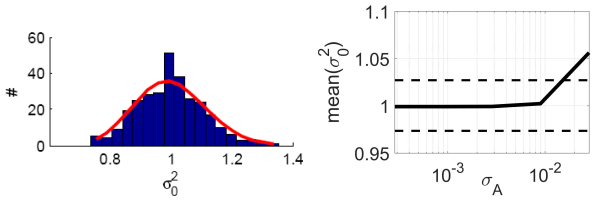

Figure 2: Evaluation of estimated variance factor. **Left:** Histogram of $K = 300$ estimated variance factors with theoretical distribution $F(144, \infty)$ overlayed, showing good correspondence. **Right:** Mean estimated variance factor as a function of the noise level. For large noise levels the nonlinearity of the model becomes slightly visible

Checking the correctness of the theoretical covariance matrix. The theoretical covariance matrix $\Sigma_{\widehat{\xi}\widehat{\xi}}$ should reflect the empirical accuracy, *i.e.* $\mathbb{E}(\underline{\Sigma_{\widehat{\xi}\widehat{\xi}}^{\text{emp}}}|H_0) = \Sigma_{\widehat{\xi}\widehat{\xi}}^{\text{theor}}$. This can be tested using a sample of simulated data leading to an empirical covariance matrix $\Sigma_{\widehat{\xi}\widehat{\xi}}^{\text{emp}}$ derived from the deviations of the estimates from their true value, see the test statistic $X^2(\text{CovM})$ which is χ^2_{15} distributed, involving, and given in [15], Sects. 2.8.7, 4.1.212.

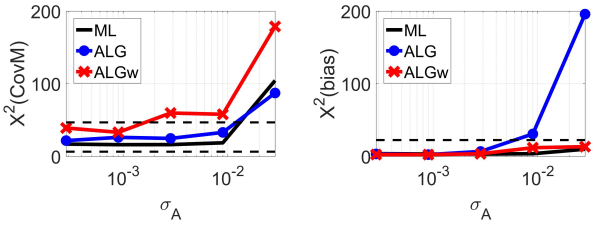

Figure 3: Test statistics for checking the covariance matrix and the mean, shown as a function of the noise level σ_A, together with the confidence regions (dashed). **Left:** Test statistic $\underline{X^2}(\text{CovM}) \sim \chi^2_{15}$ for checking the consistency of the empirical and the theoretical covariance matrix. **Right:** Test statistic $\underline{X^2}(\text{bias}) \sim \chi^2_6$ for checking the unbiasedness of the estimated parameters. For low relative accuracy, namely above 0.01 the test statistic is far outside the tolerance band

Figure 3, left, shows the test statistic $X^2(\text{CovM})$ for the covariance matrices of the maximum likelihood estimates (ML) and two of the direct solutions for a series of noise levels (ALG and ALGw). For small noise levels, below 0.3% relative precision, the hypothesis that the expected empirical covariance matrix is identical to the theoretical covariance matrix is not rejected. This also can be interpreted as follows: the theoretical covariance matrices can safely be used to predict the expected precision of the three estimation methods. Hence, also the precision of the suboptimal direct solutions can be predicted. Again, for larger noise levels, the statistical tests fire, due to the nonlinearity of the model.

Using this test for checking the correctness of the implementation (of the simulation and the estimation) turns out to be very useful, as it is a very sensitive test.

Checking the unbiasedness of the estimates. Finally, the estimation should yield values $\widehat{\boldsymbol{\xi}}$ close to the true value $\widetilde{\boldsymbol{\xi}}$. Therefore we test the hypothesis $\mathbb{E}(\underline{\widehat{\boldsymbol{\xi}}}|H_0) = \widetilde{\boldsymbol{\xi}}$. Given the covariance matrix $\Sigma_{\widehat{\xi}\widehat{\xi}}$, the estimated mean $\widehat{\boldsymbol{m}}_{\widehat{\xi}}$ of the K samples $\widehat{\boldsymbol{\xi}}_k$ of estimates should be close to $\widetilde{\boldsymbol{\xi}}$. Under the null-hypothesis, the test statistic

$$X^2(\text{bias}) = K(\widehat{\boldsymbol{m}}_{\widehat{\xi}} - \widetilde{\boldsymbol{\xi}})^\mathsf{T} \Sigma_{\widehat{\xi}\widehat{\xi}}^{-1} (\widehat{\boldsymbol{m}}_{\widehat{\xi}} - \widetilde{\boldsymbol{\xi}}) \sim \chi^2_U \qquad (31)$$

follows a χ^2_6 distribution.

Figure 3, right, shows the test statistic for a range of noise levels. Obviously, the maximum likelihood solution ML and the whitened algebraic solution ALGw, which also

takes the uncertainty of the observed planes into account, yield unbiased results over the whole range of noise levels, in contrast to the algebraic solution ALG, which for larger noise levels can be expected to be biased.

4.2. Loss in accuracy of the suboptimal solutions

We evaluate the loss in accuracy of the direct solutions using a dataset with realistic distribution of planes. The dataset consists of two point clouds captured in a lecture room, one by a Faro terrestrial laser scanner and the other by a Zeb-1 sensor. The point clouds, hereafter referred to as TLS and Zeb, were segmented into planar segments using the region growing method of Vosselman [28], resulting in 269 segments containing 4.431 million points for the TLS point cloud, and 261 segments containing 1.525 million points for the Zeb point cloud. Correspondences were found using a greedy search described in [13], yielding 57 pairs of corresponding planar segments representing 81.7% of all points. Figure 1 shows the segmented point clouds.

To evaluate the loss in accuracy of the estimation methods, we first fit planes to the segments in each point cloud and estimate the plane uncertainties using the nominal precision of the points. Based on sensor specifications, we set a nominal precision of 1.2 mm for the TLS point cloud [7] and 25 mm for the Zeb point cloud [10]. Once plane uncertainties are estimated, we find an approximate motion between the two sets of planes and treat this as the true motion. Using this true motion, the plane parameters are transformed from the Zeb frame to the TLS frame, and the covariance matrices in the TLS frame are adapted to their corresponding new plane parameters. The original and the transformed planes and their corresponding covariance matrices are treated as true observations for the estimation of motion. Then in K iterations, we perturb the planes in both sets according to their covariance matrices and estimate the motion. From the resulting discrepancies between the true motion and the estimated motion we obtain the empirical covariance matrix of the motion parameters for each solution, and evaluate the loss in accuracy of the direct solutions as compared to the optimal ML solution.

We evaluate the loss in accuracy, referring to the standard deviations of the motion parameters, namely using the following measures:

- Average loss: $\sqrt{\mathrm{tr}\left(\Sigma^{(a)}_{\widehat{\xi}\widehat{\xi}}\Sigma^{(ML),-1}_{\widehat{\xi}\widehat{\xi}}\right)/6}$,
- Maximum loss: $\sqrt{\max\lambda(\Sigma^{(a)}_{\widehat{\xi}\widehat{\xi}}\Sigma^{(ML),-1}_{\widehat{\xi}\widehat{\xi}})}$,

where $\Sigma^{(a)}_{\widehat{\xi}\widehat{\xi}}$ and $\Sigma^{(ML)}_{\widehat{\xi}\widehat{\xi}}$ denote the empricial covariance matrix of the motion estimated by the direct solution and the maximum likelihood solution, respectively.

Figure 4 shows the measures of loss in accuracy of the direct solutions for different numbers of randomly chosen plane pairs over $K = 100$ iterations. The average loss shown on the left indicates a consistently superior performance for the single-iteration ML solution (ML-1) and the whitened algebraic solution (ALGw) across different numbers of plane pairs as compared to the algebraic solution (ALG). Both solutions, ML-1 and ALGw, which exploit the uncertainty of the given plane pairs have a significantly smaller loss of accuracy as compared to ALG.

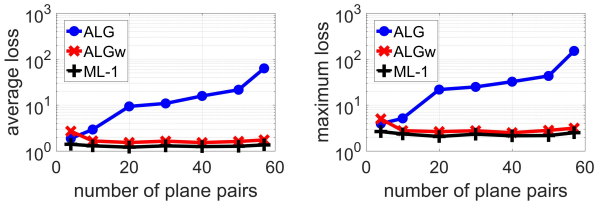

Figure 4: Loss in accuracy of the three direct solutions shown as a function of the number of plane pairs, realistic configuration, $K = 100$ iterations. **Left:** Average loss. **Right:** Maximum loss. The single iteration ML solution (ML-1) and the whitened algebraic solution (ALGw) have a significantly smaller loss of accuracy as compared to the algebraic solution (ALG) in terms of both measures

4.3. Comparison with ICP

We compare the performance of the plane-to-plane estimation methods with the classical iterative closest point (ICP) algorithm. Two variants of the ICP implemented in MATLAB®R2016 are tested: the point-to-point ICP, referred to as ICP-pt, and the point-to-plane ICP, referred to as ICP-pl, see [24]. The extrapolation-option, described in [2] is applied. To evaluate the ICP variants, we take the true plane pairs from the previous experiment and project the points in each point cloud to their corresponding true planes. Then within $K = 100$ iterations, we distort the points according to the nominal precision of the points, and apply ICP to estimate the motion. To ensure convergence, we use all 57 plane pairs, and provide as input to the ICP an initial approximation of the solution within 5 degrees and 0.1 m of the true motion. From the discrepancies between the estimated motion and the true motion over $K = 100$ iterations, we obtain the empirical covariance of the estimated motion, and compute the loss of accuracy with respect to the optimal ML solution.

Table 1 shows the result of the comparison between the direct plane-to-plane methods and the ICP variants in terms of loss of accuracy with respect to the optimal ML solution. While ICP-pl performs better than ICP-pt, both ICP variants have a significantly larger loss of accuracy as compared to ML-1 and ALGw which exploit the uncertainty of the planes.

Method	Average loss	Maximum loss
ML-1	1.24	2.04
ALGw	1.61	2.76
ALG	45.15	104.80
ICP-pl	3.66	6.09
ICP-pt	5.82	12.11

Table 1: Comparison of direct plane-to-plane methods with the point-to-point ICP (ICP-pt) and point-to-plane ICP (ICP-pl) in terms of loss of accuracy with respect to the optimal ML solution (realistic configuration, 57 plane pairs, $K = 100$ iterations)

4.4. Computation times

The estimation procedures were implemented in MATLAB. The average computation times on an Intel i7 processor with 2.70 GHz speed and 8 GB memory for different estimation methods using plane-to-plane correspondences are given in Table 2. The computation times for 1000 (randomly generated) plane pairs shows that the estimation methods can be scaled up to larger scenes with more planes and perform in real time. However, – out of the scope of this paper – the prerequisite steps, segmentation and search for plane correspondences, are expensive processes. The segmentation process took 352 seconds for the TLS point cloud with 4.4 million points and 106 seconds for the Zeb point cloud with 1.5 million points using the software by G. Vosselman [28].

The search for correspondences took 225 seconds to find 57 plane pairs. This indicates that for practical plane-to-plane registration of point clouds more efficient segmentation and correspondence search methods should be used. Also, the ICP registration of the two point clouds with the used MATLAB-tools are comparably slow, and took on average 299 and 934 seconds respectively for the ICP-pl and ICP-pt variants.

# pairs	ML	ML-1	ALGw	ALG
57	0.085	0.012	0.021	0.010
1000	1.6247	0.1331	0.3088	0.0653

Table 2: CPU times (in seconds) for the optimal and direct motion estimation methods for 57 and 1000 plane pairs

5. Registering multiple point clouds

The registration of multiple point clouds based on pairwise matches of planes can exploit the derived constraints to advantage. Assume, we have F frames, *i.e.* motions $\mathcal{M}_f$, one of them acting as reference frame. Let the scene have P planes $\mathcal{A}_p$, which are unknown and serve as link between the frames via Q observed planar regions $\mathcal{A}_q := \mathcal{A}_p^f$ with $q = (p, f)$. Finally we assume we have found C correspondences $c = (p, f, p', f')$ between planes $\mathcal{A}_p^f$ and $\mathcal{A}_{p'}^{f'}$. Then, starting from approximate values for the motions and the scene planes, the task is to find estimates for the corrections $\Delta\boldsymbol{\xi}_f$ of the unknown motions and the corrections $\Delta\boldsymbol{A}_{rp}$ to the unknown planes such that

$$\Omega\left(\{\widehat{\Delta\boldsymbol{\xi}_f}\};\{\widehat{\Delta\boldsymbol{A}_{rp}}\}\right) = \sum_q ||\widehat{\boldsymbol{v}}_{A_{rp}^f}||^2_{\Sigma_{A_{rp}^f A_{rp}^f}} \qquad (32)$$

is minimized under the constraints $g_c(\mathsf{M}_{ff'}; \mathbf{A}_p^f, \mathbf{A}_{p'}^{f'}) = \mathbf{0}$ for all $c = 1, ..., C$. Observe, in contrast to the setup in (12), where each constraint refers to exactly one plane in both frames, here we allow for arbitrary matches, *i.e.* each obseved plane in one frame may match several planes in other frames. Therefore, the classical optimization criterion used in SLAM, see [16] or [31], which minimizes the alternative objective function

$$\Omega'\left(\{\widehat{\Delta\boldsymbol{\xi}_f}\}\right) = \sum_c ||g_c(\mathsf{M}_{ff'}; \mathbf{A}_p^f, \mathbf{A}_{p'}^{f'})||^2_{\Sigma_{g_c g_c}} \qquad (33)$$

with respect to the unknown motions, is suboptimal, for two reasons: (1) since observed planes correspond to several planes, the constraint residuals g_c are not mutually independent, which is not taken into account in (33); (2) the observed plane parameters are fixed and not corrected, to achieve fitted plane parameters. Following the investigations in [25], case C, the loss in precision can be expected to be below a factor 1.5, which however needs to be verified.

Again, the method can be made robust w.r.t. wrong correspondences, as *e.g.* in [31], namely, by iteratively reweighting the residual, hence to replace the weighted sum of squares by a robust minimization function $\sum_q \rho\left(||\widehat{\boldsymbol{v}}_{A_{rp}^f}||_{\Sigma_{A_{rp}^f A_{rp}^f}}\right)$.

6. Outlook

The paper presents new optimal and suboptimal direct solutions for determining the relative motion of point clouds based on plane-to-plane correspondences. The estimates are computationally efficient, allowing real time performance. The new direct methods, which take the uncertainty of the given plane pairs into account only show a small loss, below a factor 3 compared to the statistically optimal estimate. The whitened algebraic solution allows to predict the precision of the estimated motion which can be used within a SLAM procedure. The proposed methods are faster and more precise than classical ICP methods. Future work refers to exploiting the uncertainty of the extracted planes for efficiently establishing correspondences and investigating the performance of multi-frame estimates.

Acknowledgments: We appreciate the use of the software for point cloud segmentation of G. Vosselman [28].

References

[1] K. Al-Durgham, A. Habib, and M. Mazaheri. Solution Frequency-Based Procedure for Automated Registration of Terrestrial Laser Scans Using Linear Features. In *Proc. of Ann. Conf.of the American Society for Phtogrammetry and Remote Sensing*, 2014. 2

[2] P. J. Besl and N. McKay. A method for registration of 3-D shapes. *IEEE Transactions on Pattern Analysis and Machine Intelligence*, 14(2):239–256, 1992. 1, 7

[3] S. D. Billings, E. M. Boctor, and R. H. Taylor. Iterative Most-Likely Point Registration (IMLP): A Robust Algorithm for Computing Optimal Shape Alignment. *PLOS ONE*, 10(3):e0117688, 2015. 1

[4] C. Brenner, C. Dold, and N. Ripperda. Coarse orientation of terrestrial laser scans in urban environments. *ISPRS Journal of Photogrammetry and Remote Sensing*, 63(1):4–18, 2008. 2

[5] Y. Chen and G. Medioni. Object modeling by registration of multiple range images. *Image and Vision Computing*, 10(3):145–155, 1992. 1

[6] E. Eade. Lie Groups for 2D and 3D Transformations. http://ethaneade.com/lie_groups.pdf, last visited 2.6.2016, 2014. 3

[7] Faro. Faro focus technical specifications. 7

[8] W. Förstner. A Feature Based Correspondence Algorithm for Image Matching. In *Intl. Archives of Photogrammetry and Remote Sensing*, volume 26, pages 150–166. ISP Symposium, Comm. III, Rovaniemi, 1986. 4

[9] W. Förstner and B. P. Wrobel. *Photogrammetric Computer Vision – Statistics, Geometry, Orientation and Reconstruction*. Springer, 2016. 2, 3, 5

[10] GeoSLAM. Zeb1 - handheld mobile mapping system. 7

[11] J. Gregor and R. T. Whitaker. Indoor scene reconstruction from sets of noisy range images. *Graphical Models*, 63(5):304–332, 2001. 2

[12] D. Holz, S. Holzer, R. B. Rusu, and S. Behnke. *Real-Time Plane Segmentation Using RGB-D Cameras*, pages 306–317. Springer Berlin Heidelberg, 2012. 2

[13] K. Khoshelham. Automated Localization of a Laser Scanner in Indoor Environments Using Planar Objects. In *International Conference on Indoor Positioning and Indoor Navigation (IPIN)*, Zürich, Switzerland, 2010. 2, 7

[14] K. Khoshelham. Closed-form solutions for estimating a rigid motion from plane correspondences extracted from point clouds. *ISPRS Journal of Photogrammetry and Remote Sensing*, 114:78–91, Apr. 2016. 1, 4

[15] K.-R. Koch. *Parameter Estimation and Hypothesis Testing in Linear Models*. Springer, 2nd edition, 1999. 6

[16] R. Kümmerle, G. Grisetti, H. Strasdat, K. Konolige, and W. Burgard. g2o: A General Framework for Graph Optimization. In *Proc. of the IEEE Int. Conf. on Robotics and Automation (ICRA)*, Shanghai, China, 2011. 8

[17] D. D. Lichti and J. C. K. Chow. Inner Constraints for Planar Features. *The Photogrammetric Record*, 28(141):74–85, 2013. 1

[18] L. Maier-Hein, A. M. Franz, T. R. d. Santos, M. Schmidt, M. Fangerau, H. P. Meinzer, and J. M. Fitzpatrick. Convergent Iterative Closest-Point Algorithm to Accomodate Anisotropic and Inhomogenous Localization Error. *IEEE Transactions on Pattern Analysis and Machine Intelligence*, 34(8):1520–1532, 2012. 1

[19] N. J. Mitra, N. Gelfand, H. Pottmann, and L. Guibas. Registration of point cloud data from a geometric optimization perspective. In *Proceedings of the 2004 Eurographics/ACM SIGGRAPH Symposium on Geometry Processing*, pages 22–31. ACM, 2004. 1

[20] K. Pathak, A. Birk, N. Vaskevicius, and J. Poppinga. Fast Registration Based on Noisy Planes With Unknown Correspondences for 3-D Mapping. *IEEE Transactions on Robotics*, 26(3):424–441, 2010. 2

[21] K. Pathak, N. Vaskevicius, and A. Birk. Uncertainty analysis for optimum plane extraction from noisy 3D range-sensor point-clouds. *Intelligent Service Robotics*, 3(1):37, 2009. 2

[22] M. Poreba and F. Goulette. A Robust Linear Feature-Based Procedure for Automated Registration of Point Clouds. *Sensors*, pages 1435–1457, 2015. 2

[23] S. Ramalingam and Y. Taguchi. A Theory of Minimal 3D Point to 3D Plane Registration and Its Generalization. *International Journal of Computer Vision*, 102(1-3):73–90, 2013. 1

[24] S. Rusinkiewicz and M. Levoy. Efficient Variants of the ICP Algorithm. In *Third International Conference on 3-D Digital Imaging and Modeling*, 2001. 7

[25] J. Schneider, C. Stachniss, and W. Förstner. On the quality and efficiency of approximate solutions to bundle adjustment with epipolar and trifocal constraints. In *Proceedings of the ISPRS Conference on Unmanned Aerial Vehicles in Geomatics (UAV-g)*, 2017. 8

[26] A. Segal, D. Haehnel, and S. Thrun. Generalized-ICP. In *Proceedings of Robotics: Science and Systems*, 2009. 1

[27] G. Taubin. An Improved Algorithm for Algebraic Curve and Surface Fitting. In *Fourth International Conference on Computer Vision, Berlin*, pages 658–665, 1993. 5

[28] G. Vosselman. Point cloud segmentation for urban scene classification. *ISPRS - International Archives of the Photogrammetry, Remote Sensing and Spatial Information Sciences*, (2):257–262, Oct. 2013. 7, 8

[29] J. Xiao, B. Adler, and H. Zhang. 3D Point Cloud Registration Based on Planar Surfaces. In *Conf. on Multisensor Fusion and Integration for Intelligent Systems*, pages 40–45, 2012. 2

[30] J. Xiao, J. Zhang, J. Zhang, H. Zhang, and H. P. Hildre. Fast plane detection for SLAM from noisy range images in both structured and unstructured environments. In *International Conference on Mechatronics and Automation*, pages 1768–1773, 2011. 2

[31] Q.-Y. Zhou, J. Park, and V. Koltun. Fast Global Registration. In *Proc. Europ. Conf. on Computer Vision*, 2016. 4, 8